Analysis of fuel rod behavior during loss-of-coolant accidents using the BISON code: Cladding modeling developments and simulation of separate-effects experiments

G. Pastore [a],[1],[*], R.L. Williamson [a], R.J. Gardner [a],[2], S.R. Novascone [a], J.B. Tompkins [b], K.A. Gamble [a], J.D. Hales [a]

[a] Idaho National Laboratory, Computational Mechanics and Materials Department, P.O. Box 1625, Idaho Falls, ID 83415-3840, United States
[b] Texas A&M University, Department of Nuclear Engineering, 3133 TAMU, College Station, TX 77843-3133, United States

ARTICLE INFO

ABSTRACT

BISON is a finite-element based, multidimensional fuel performance code developed at Idaho National Laboratory. In this paper, we present BISON modeling developments for Zircaloy nuclear fuel cladding behavior under loss-of-coolant accident (LOCA) conditions and code validation to separate-effects experiments. Code developments include models for cladding high-temperature creep, crystallographic phase transition, high-temperature steam oxidation and failure due to burst. Code validation is performed against a substantial number of experimental tests for ballooning and burst behavior of Zircaloy claddings under LOCA conditions. Validation calculations are completed using 2D axisymmetric models. Additionally, we present a 3D calculation that demonstrates simulation of the cladding response in presence of azimuthal temperature variations. Calculated results are systematically compared to experimental data of cladding temperature, inner pressure and time at burst failure. Several of the presented BISON validation cases were developed in the framework of the IAEA Coordinated Research Project FUMAC. BISON modeling developments for UO_2 fuel behavior under LOCA conditions and code validation to integral fuel rod experiments are presented in a complementary paper.

© 2020 Elsevier B.V. All rights reserved.

1. Introduction

Developing computational tools able to reliably assess the thermo-mechanical behavior and integrity of the nuclear fuel rods in the reactor during accidents is essential from both safety and economic standpoints. For this purpose, increasingly complex and efficient fuel performance codes are developed. In the past, separate codes have been employed for analyzing normal operating and accidental reactor conditions, which can lead to difficulties with code coupling and management. Developing codes able to deal with both domains is desirable, yet it calls for the implementation of specific models dealing with the additional physics and increased complexity that characterize fuel rod behavior during accident situations relative to normal operating conditions [1–3].

In particular, postulated loss-of-coolant accident (LOCA) conditions form the basis for many design considerations in light water reactors (LWRs). During the heat-up phase of a LOCA, the fuel cladding temperature increases, normally at a rate of a few degrees per second in the earlier phase of the temperature escalation. With increasing temperature and depressurization of the reactor vessel, the Zr-based cladding becomes more and more prone to viscoplastic (creep) outward deformation under the effect of the rod inner pressure. Also, the cladding oxidizes rapidly in a high-temperature steam environment, leading to a positive temperature feedback as a consequence of the additional thermal resistance due to the outer oxide layer, and to a thinning of the metallic wall resulting in higher stresses and creep rates. A fraction of the hydrogen produced during the oxidation reaction is picked up by the cladding, and affects the cladding residual ductility after cooling below the Zr hydride precipitation temperature. Moreover, the

---

* Corresponding author.

E-mail addresses: gpastore@utk.edu (G. Pastore), richard.williamson@inl.gov (R.L. Williamson), rgardner@kairospower.com (R.J. Gardner), stephen.novascone@inl.gov (S.R. Novascone), tompkins@tamu.edu (J.B. Tompkins), kyle.gamble@inl.gov (K.A. Gamble), jason.hales@inl.gov (J.D. Hales).

[1] Current address: University of Tennessee, Department of Nuclear Engineering, 1412 Circle Dr, Knoxville, TN 37916, United States.

[2] Current address: Kairos Power L.L.C., 707 W Tower Ave, Alameda, CA 94501, United States.

Zr-based cladding alloy undergoes a crystallographic phase transition from hexagonal (α-phase) to cubic (β-phase) crystal structure at temperatures exceeding about 1000-1100 K, although the onset temperature for the transition is affected by the heating rate and amounts of hydrogen and oxygen contained in the metallic wall. The phase transition affects the cladding creep rate. Thermal creep during the LOCA transient results in cladding ballooning in the space between the fuel assembly grid spacers and may ultimately cause cladding failure due to burst, breaking the first barrier of radiation containment. Cladding resistance to burst failure is affected by both oxygen uptake in the metal during oxidation and crystallographic phase transition [4]. Clearly, all of these phenomena, and their mutual interactions, need to be covered in computational models for reliably evaluating fuel rod performance during LOCA accidental situations.

Fuel performance code developments enabling the simulation of both normal operating and LOCA conditions have been presented, e.g., in [1,5,6]. The need for adequate fuel performance modeling during postulated LOCAs is confirmed by the organization of international collaboration projects on this subject, such as the recently concluded Coordinated Research Project (CRP) on Fuel Modeling in Accident Conditions (FUMAC) of the International Atomic Energy Agency (IAEA) [7]. The FUMAC project has involved a benchmark of various fuel performance codes for LWR fuel rod behavior analysis under LOCA conditions based on a set of experimental cases. The project has resulted in an assessment of the state of the art of fuel modeling during LOCA accidents. Among the main conclusions, it was noted that a significant dispersion still exists among the calculations for the time to cladding burst failure from different codes. It was also evident that the evaluation of cladding strain at burst is subject to large uncertainties, which is mainly related to the high cladding strain rates reached as burst is approached and the uncertainties in the cladding deformation and burst models, but also to the uncertainties pertaining to the experimental data. Another issue that was identified relates to the dimensionality of the problem. While fuel performance codes often approximate fuel rod behavior with axially-stacked 1D (so-called 1.5D) or 2D axisymmetric representations, 3D aspects such as the effects of azimuthal temperature variations in the cladding can be important under LOCA conditions.

BISON [8] is a finite-element based, multidimensional fuel performance code developed at Idaho National Laboratory (INL). Initially, BISON verification and validation has focused on LWR fuel during normal operating conditions [9,10]. More recently, code development and validation work for the analysis of LOCA accident scenarios has been performed. BISON includes a large-strain mechanics formulation, essential to correctly analyze cladding ballooning during LOCAs. In order to capture the complex material response during accident situations, however, it is also necessary to implement specific models for the high-temperature, transient phenomena involved. For this purpose, dedicated material models have been incorporated in the thermo-mechanics analysis framework of the code. In this paper, first, models added to BISON that are specific to cladding behavior under LOCA conditions are overviewed. These code developments focus on the high-temperature behavior of Zircaloy cladding and include, in particular, models for steam oxidation, crystallographic phase transition, creep deformation and failure due to burst. Second, we give an account of code validation to out-of-pile, separate-effects cladding ballooning and burst experiments. Analyzed validation cases include a substantial number of tests from the REBEKA [4,11,12], PUZRY [13,14], Hardy [15], ORNL [16] and QUENCH-L1 [17] experimental series. All calculations were performed using 2D axisymmetric models. Additionally, for one of the REBEKA cases we present a 3D calculation that demonstrates simulation of the cladding response in presence of azimuthal temperature varia-

tions. Several of the presented BISON validation cases were developed in the framework of INL's participation in the IAEA FUMAC project [7].

To perform integral fuel rod analyses, in addition to the cladding modeling developments presented in this paper, fuel modeling developments are necessary. In the second part of this work [18], we present BISON developments for UO₂ fuel behavior under LOCA conditions and validation of the extended code to integral fuel rod LOCA tests.

The outline of the paper is as follows. Section 2 summarizes the BISON modeling developments for Zircaloy cladding behavior under LOCA conditions. Section 3 presents code validation to cladding ballooning and burst tests. Conclusions are presented in Section 4.

2. Cladding modeling developments

2.1. High-temperature steam oxidation

Oxidation of Zr-based cladding through reaction with the coolant affects both thermal and mechanical performance of the cladding. First, the growth of a zirconium dioxide (ZrO₂) layer on the cladding outer surface adds to the thermal resistance to heat transfer from the fuel to the coolant and leads to thinning of the metallic wall. Second, oxygen uptake into the metal affects the mechanical properties and burst failure behavior of the cladding. Third, the exothermic oxidation reaction leads to energy deposition to the cladding, further contributing to the temperature escalation during a LOCA. High-temperature steam oxidation proceeds much more rapidly than oxidation at normal LWR operating temperatures. Under high-temperature conditions, the kinetics of oxide layer growth and oxygen mass gain can be described by a parabolic law, with the reaction rate constant defined as a function of temperature through an Arrhenius relation [19]:

$$\frac{d\xi^2}{dt} = A \exp\left(\frac{-Q}{RT_I}\right) \tag{1}$$

where ξ is either the oxide layer thickness, $\xi = s$ (m), or the gained oxygen mass, $\xi = g$ (kg $\times$ m^{-2}), T_I (K) the metal-oxide interface temperature, A (m²s^{-1} or kg $\times$ m^{-2}) the oxidation rate constant, Q (J $\times$ mol^{-1}) the activation energy, and R (J $\times$ mol^{-1}K^{-1}) the universal gas constant.

For the parameters in the correlation given by Eq. 1, the BISON model includes values for either oxide layer growth or oxygen mass gain applicable to Zircaloy-2/4 and appropriate to different temperature ranges. In particular, in line with the recommendation in [19], the following approach is adopted:

- For metal-oxide interface temperatures from 673 K to 1800 K, the Leistikow [20] correlation is used. The Cathcart–Pawel correlation [21] is also available as an option. The Leistikow correlation has been selected as reference in view of the larger underlying database, the availability of experimentally determined mass gain for all considered tests, and the better fit in the lower temperature region relative to the Cathcart–Pawel correlation [19].
- Above 1900 K, the Prater–Courtright correlation [22] is used.
- Between 1800 and 1900 K, a linear interpolation between the Leistikow (or Cathcart–Pawel) and Prater–Courtright correlations is made. Linear interpolation between two correlations of Arrhenius type is obtained by a third correlation of the same type [19].

The values for the parameters in Eq. (1) relative to the different correlations are given in Table 1.

For normal operating temperatures, i.e., below 673 K, the EPRI/KWU/C-E oxidation model [23,24] is used in BISON.

Table 1
Parameters of the correlations for oxide layer thickness (*s*) and oxygen mass gain (*g*) at high temperature [19].

Correlation	A_s (m^{2}s^{-1})	$\frac{Q_s}{R}$ (K)	A_g (kg × m^{-2})	$\frac{Q_g}{R}$ (K)
Leistikow	7.82×10^{-6}	20214	52.42	20,962
Cathcart-Pawel	2.25×10^{-6}	18062	36.22	20,100
Prater-Courtright	2.98×10^{-3}	28420	3.3×10^3	26,440

It should be mentioned that in the BISON analysis, while the effect of the oxide layer is accounted for in terms of an additional thermal resistance to heat transfer to the coolant, the thinning of the metallic wall during oxide growth is not considered. This would require modifying the finite element mesh during the simulation to introduce a moving metal-oxide interface (e.g., using the extended finite element method [25,26]). Such a capability is currently not available in BISON, but is of interest as a future development.

2.2. Crystallographic phase transition

Above temperatures of 1000–1100 K, approximately, time-dependent phase transformation of zirconium alloys from hexagonal (α-phase) to cubic (β-phase) crystal structure occurs. Modeling the kinetics of crystallographic phase transformation is pivotal for the assessment of cladding mechanical behavior and integrity (creep deformation and burst) during a postulated LOCA.

A model has been implemented in BISON for the calculation of the volume fraction of β phase over the total volume of material as a function of time and temperature during phase transformation in non-isothermal conditions. The model is based on [27–29] and relates to data for Zircaloy-4. The phase transformation rate is expressed by

$$\frac{dy}{dt} = k(T)[y_s(T) - y] \tag{2}$$

where *y* (/) is the volume fraction of β-phase, *t* (s) the time, y_s (/) the steady-state or equilibrium value of *y*, *k* (s^{-1}) the rate parameter, and *T* (K) the temperature. The volume fraction of β-phase at equilibrium is represented by a sigmoid function of temperature

$$y_s = \frac{1}{2}\left[1 + \tanh\left(\frac{T - T_{cent}}{T_{span}}\right)\right] \tag{3}$$

where T_{cent} and T_{span} are material-specific parameters related to the center and span of the mixed-phase temperature region, respectively. For Zircaloy-4, $T_{cent} = 1159 - 0.096w$ (K) and $T_{span} = 44 + 0.026w$ (K) [27] are used, with *w* being the hydrogen concentration in the range $0 \leq w \leq 1000$ wppm (weight parts per million hydrogen). The rate parameter is expressed in the form

$$k = k_0 \exp\left[-\frac{E}{k_b T(t)}\right] + k_m \tag{4}$$

where k_0 is a kinetic prefactor, *E* an effective activation energy, k_b the Boltzmann constant, and k_m a constant. For Zircaloy-4, $k_0 = 60,457 + 18,129|\dot{T}|$ (s^{-1}) and $\frac{E}{k_b} = 16,650$ (K) [27,29] are used, where $\dot{T} = \frac{dT}{dt}$ (Ks^{-1}) is the heating rate in the range $0.1 \leq |\dot{T}| \leq 100 \, Ks^{-1}$. The α → β transformation is purely diffusion controlled, while the β → α transformation is partly martensitic. This is represented by the constant k_m given in the form [29]

$$\begin{cases} k_m = 0 & \alpha \rightarrow \beta \\ k_m = 0.2 & \beta \rightarrow \alpha \end{cases} \tag{5}$$

The starting temperatures for the onset of $\alpha \rightarrow \alpha + \beta$ and $\beta \rightarrow \alpha + \beta$ phase transformations are calculated as [27]
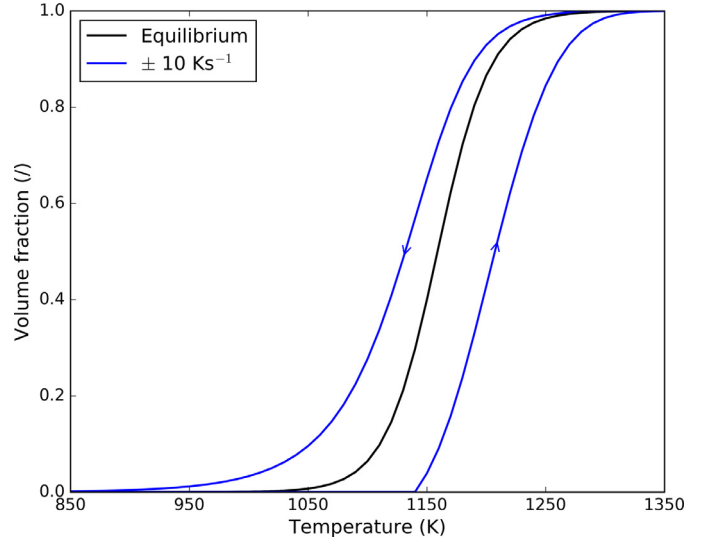

Fig. 1. Calculated volume fraction of β phase as a function of temperature. Equilibrium conditions (slow temperature variation) and temperature variation rates of ± 10 Ks^{-1} are included.

$$T_{\alpha \rightarrow \alpha + \beta} = \begin{cases} 1083 - 0.152w & \text{for } 0 \leq \dot{T} < 0.1 \text{ Ks}^{-1} \\ (1113 - 0.156w)\dot{T}^{0.0118} & \text{for } 0.1 \leq \dot{T} \leq 100 \text{ Ks}^{-1} \end{cases} \tag{6}$$

$$T_{\beta \rightarrow \alpha + \beta} = \begin{cases} 1300 & \text{for } -0.1 < \dot{T} \leq 0 \text{ Ks}^{-1} \\ 1302.8 - 8.333|\dot{T}|^{0.477} & \text{for } -100 \leq \dot{T} \leq -0.1 \text{ Ks}^{-1} \end{cases} \tag{7}$$

where $T_{\alpha \rightarrow \alpha + \beta}$ and $T_{\beta \rightarrow \alpha + \beta}$ are in K. For the calculations performed in this work and presented in Section 3, in the absence of a hydrogen pickup model validated for LOCA conditions in BISON at this time, the effect of hydrogen on the phase transition behavior is not included, i.e., $w = 0$ is considered. Accounting for hydrogen effects in cladding behavior under LOCA conditions is an important aspect for the future development of BISON.

The β-phase volume fraction as a function of time is calculated by numerical integration of Eq. (2). The calculated volume fraction of β phase as a function of temperature at equilibrium and for temperature variation rates of ± 10 Ks^{-1} is shown in Fig. 1.

2.3. High-temperature creep

During a LOCA, outward creep deformation of the cladding tube under the effect of internal pressurization and high temperature leads to cladding ballooning and eventual failure due to burst. The model available in BISON for high-temperature creep of Zircaloy claddings is the one from [4,30]. The steady-state creep rate is defined by a correlation in the form of a Norton power equation:

$$\dot{\epsilon}_{eff} = A \times \exp\left(\frac{-Q}{RT}\right)\sigma_{eff}^n \tag{8}$$

where $\dot{\epsilon}_{eff}$ (s^{-1}) is the effective creep strain rate, *A* (MPa^{-n}s^{-1}) the strength coefficient, *Q* (J/mol) the activation energy for the creep deformation, *T* (K) the temperature, σ_{eff} (MPa) the effective (Von Mises) stress, and *n* (/) the stress exponent. Given the above creep rate equation, at each time step, the stress-strain problem is solved implicitly. The material parameters (Table 2) used in the model were obtained from tension tests on Zircaloy-4 tubes [4,30]. In the mixed phase (α + β) region, interpolations are made to calculate

Table 2

Values for the parameters in the correlation for high-temperature creep of Zircaloy [4,11].

Phase	$\dot{\epsilon}_{eff}$ (s^{-1})	A (MPa^{-n}s^{-1})	Q (J/mol)	n (/)
α	any	19370	$3.21 \times 10^5 + 24.69 \times (T - 923.15)$	5.89
50%α–	$\leq 3 \times 10^{-3}$	0.24	1.02×10^5	2.33
50%β	$> 3 \times 10^{-3}$	Lin. interp. $\ln(A)$	Lin. interp	Lin. interp.
β	any	7.9	1.42×10^5	3.78

the Norton parameters. Depending on the strain rate, different approaches are adopted [30]:

- For $\dot{\epsilon}_{eff} \leq 3 \times 10^{-3}$ s^{-1}, linear interpolation of $\ln(A)$, n, and Q is made between the values for pure α and middle of $\alpha + \beta$ (50%α–50%β) phase, and between 50%α–50%β and pure β phase.
- For $\dot{\epsilon}_{eff} > 3 \times 10^{-3}$ s^{-1}, it is assumed that the values of $\ln(A)$, n, and Q vary linearly between the values for pure α and pure β phase.

To perform the interpolation, the fraction of each phase calculated by the phase transition model described in Section 2.2 is used.

It must be noted that while Eq. (8) refers to the steady-state creep rate [4,30], in this work, it is used to represent the overall plastic strain of the cladding under LOCA conditions (ballooning). This assumption is consistent with the work on deriving burst failure criteria by the developers of the creep model in [4,30]. As commented in [30], the assumption is stronger at large strains approaching the burst strain.

It also must be noted that according to the considered sources, creep of Zircaloy in the pure α phase is anisotropic [4,30] and that only treatment of isotropic inelastic deformation behavior is available in BISON. This is an implication of the numerical iteration algorithm used for the update of the stress tensor in presence of an inelastic strain increment (return mapping algorithm), which underlies the assumption of isotropic behavior [31]. To the best of our knowledge, the rigorous treatment of anistoropic high-temperature creep of Zircaloy in fuel performance codes is still an open issue. This general problem has also been identified during the recent IAEA FUMAC project [7]. Arguably, this is an important limitation for fuel performance analysis during LOCAs, and the extension of BISON to enable a rigorous treatment of anisotropic strain is planned as a next step of code development.

2.4. Burst failure criteria

For determining the conditions for failure due to burst of Zircaloy cladding under LOCA conditions, the following criteria have been implemented in BISON:

1. An overstress criterion, which assumes that burst occurs when the local hoop stress equals a limiting burst stress, i.e. [4,30]:

$$\sigma_{\theta} \geq \sigma_b \tag{9}$$

where σ_{θ} (MPa) is the hoop stress and σ_b (MPa) the burst stress.

2. An overstrain criterion, which considers the cladding to have failed when the permanent hoop strain exceeds a limiting value:

$$\epsilon_{\theta} \geq \epsilon_b \tag{10}$$

where ϵ_{θ} is the (true) hoop strain and ϵ_b is the limiting value. Following [32], we use $\epsilon_b = 33.6\%$ true strain, corresponding to value of 40% for the engineering strain.

3. A plastic strain rate criterion, which considers cladding burst at the attainment of a limiting value for the effective plastic strain

Table 3

Values for the parameters in the correlation for the burst stress of Zircaloy [4].

Phase	a (MPa)	b (K^{-1})
α	830	1×10^{-3}
50%α–50%β	3000	3×10^{-3}
β	2300	3×10^{-3}

rate:

$$\dot{\epsilon}_{pl,eff} \geq \dot{\epsilon}_b \tag{11}$$

where $\dot{\epsilon}_{pl,eff}$ is the effective plastic (creep + plasticity) strain rate and $\dot{\epsilon}_b$ is the limiting value. Following [32], we choose $\dot{\epsilon}_b = 100$ h$^{-1} \cong 2.78 \times 10^{-2}$ s^{-1}.

4. A combination of the overstress and overstrain criteria, which establishes that cladding burst occurs when either condition expressed by Eq. (9) or Eq. (10) is fulfilled.

5. A combination of the overstress and plastic strain rate criteria, which establishes that cladding burst occurs when either condition expressed by Eq. (9) or Eq. (11) is fulfilled.

The calculation of the burst stress used in Eq. (9) follows the work of Erbacher et al. [4] and is based on data from Zircaloy-4 cladding burst tests. The burst stress depends on the temperature and oxygen concentration in the cladding and is calculated as [4]:

$$\sigma_b = a \times \exp\left(-bT\right) \exp\left[-\left(\frac{\eta - \eta_0}{9.5 \times 10^{-4}}\right)^2\right] \tag{12}$$

where a (MPa) and b (K^{-1}) are constants determined experimentally and that depend on the crystallographic phase of the material, η (/) is the oxygen weight fraction in the cladding, and η_0 the oxygen weight fraction at fabrication. Eq. (12) was derived based on experiments performed on fresh claddings, hence, only the oxygen uptake during the LOCA event was considered [4]. It should also be mentioned that the burst stress for Zircaloy-4 alloys of more recent fabrication than that considered in [4] may be different, e.g., due to differences in alloy composition and anisotropy coefficients.

The values for the constants a and b in Eq. (12) are given in Table 3. In the mixed phase ($\alpha + \beta$) region, linear interpolations of $\ln(a)$ and b are made between the values for pure α and 50α–50%β phase, and between 50%α–50%β and pure β phase [4]. The volume fractions of each phase are calculated using the phase transformation model described in Section 2.2. A value $\eta_0 = 1.2 \times 10^{-3}$ for the oxygen weight fraction at fabrication is considered [4]. The current oxygen weight fraction is computed based on the oxygen mass gain from the oxidation model (Section 2.1) as

$$\eta = \frac{2r_{cl,o}}{\rho_{Zry}\left(r_{met,o}^2 - r_{cl,i}^2\right)}g + \eta_0 \tag{13}$$

where $r_{cl,o}$ (m) is the cladding outer radius, ρ_{Zry} (kg $\times$ m^{-3}) the density of the cladding metal, $r_{cl,i}$ (m) the cladding inner radius, g (kg $\times$ m^{-2}) the oxygen mass, and $r_{met,o} = r_{cl,o} - s/R_{PB}$, with s (m) being the oxide layer thickness and $R_{PB} = 1.56$ the Pilling–Bedworth ratio for Zr.

It has been noted that the overstress criterion may lead to non-conservative evaluations in low-stress situations, and that a combination with a criterion limiting the total strain or strain rate is thus preferable [32]. Following [32], in this work, we apply the combined overstress and overstrain criterion to estimate the condition of cladding burst failure.

Also, as mentioned above, the formulation for the burst stress (Eq. (12)) is based on data from fresh cladding experiments [4]. When applied to BISON simulations involving pre-irradiation before the LOCA transient, the burst stress approach has been found to be inadequate as it leads to early cladding failure in the simulations, due to an excessively low burst stress in presence of pre-LOCA oxidation. Accordingly, while we apply the combined criterion to simulations presented in this paper as they are limited to fresh cladding behavior, we consider the pure overstrain criterion in cases involving pre-irradiation [18].

3. Validation to separate-effects experiments

The BISON code, extended with the modeling capabilities described in Section 2, was tested through simulation of dedicated out-of-pile, separate-effects experiments (i.e., not including nuclear fuel pellets) of cladding ballooning and burst under representative LOCA conditions. The purpose was to assess the fidelity of the combined application of the new material models in reproducing cladding behavior, decoupled from complexities related to the calculation of cladding boundary conditions that are dependent on fuel behavior. Such separate-effects validation was comprised of simulations of 72 cladding tests from five experimental series, as summarized in Table 4.

The large-strain mechanics formulation of BISON was applied in all simulations. Using a large-strain mechanics formulation is important to correctly analyze cladding ballooning, as discussed, e.g., in [32]. Following solution verification with varying mesh refinement levels, 20-80 axial elements and 1-8 radial elements were used for the cladding, depending on the specific simulated test series. The numerical error due to time discretization was controlled by an automatic time step criterion based on limitation of the maximum inelastic strain increment during a time step [33].

The following sections present the simulations for each of the experimental series and the comparisons to experimental data, with a focus on burst failure conditions in terms of time and cladding temperature and pressure. Comparisons to cladding burst strain data are not included in the present validation study. This choice is related to:

- The adoption of a failure criterion that involves a strain limit (Eq. (10)), for which the peak strain at burst is effectively imposed. Most of the experimental strain data for the cases considered in this work are limited to the peak strain rather than including detailed axial profiles.
- The uncertainties related to the interpretation of some of the experimental data for the peak strain at burst, such as the question of whether the burst opening was considered in the reported values [7,34].

Comparisons of BISON calculations to experimental data of cladding strain for integral fuel rod LOCA experiments, where detailed information on the axial strain profile is available, are presented in the second part of this work [18]. Also, comparisons of BISON calculations of cladding strains and other fuel performance parameters to experimental data and calculations from other codes for further LOCA experimental tests are presented in [35].

3.1. REBEKA experimental series

The REBEKA experimental series [4,11,12] was carried out at Kernforschungszentrum Karlsruhe with the purpose to establish data of cladding ballooning and burst with reference to LOCA conditions. The tests were performed on single PWR-type Zircaloy-4 cladding tube samples subject to temperature transients in steam at a variety of internal pressures and heating rates. In this section, BISON simulations of the tests from the REBEKA program are presented. Simulations include 2D analyses as well as a 3D demonstration analysis.

3.1.1. Description of the tests

The cladding tubes had fabricated inner and outer diameters of 9.30 and 10.75 mm, respectively, with a 325 mm heated length, and were heated from the inside using an electrically insulated heater rod. A stack of Al_2O_3 annular pellets surrounding the heater was used as surrogate fuel. The radial gap between the cladding inner diameter and the pellet outer diameter was 75 μm. The test parameters covered a range of 1 to 14 MPa for the internal rod (helium) pressure and 1 to 35 Ks^{-1}, approximately, for the heating rate. The test atmosphere was almost stagnant steam at atmospheric pressure and at a temperature of 473 K. The cladding temperatures were measured by thermocouples spot-welded on the outer surface of the cladding. More details on the experimental apparatus and conditions are given in [4,11,12].

3.1.2. Setup of BISON simulations

The BISON geometric models of the REBEKA rods were constructed only including the cladding, while the internal electric heating and the presence of the Al_2O_3 pellets were simulated by a time-dependent Dirichlet temperature boundary condition applied to the tube inner wall. For simplicity, only the heated portion of the rods was simulated. As a result of the uniform axial power generation in the heater rod [12], the developed thermal boundary condition consists of a parabolic temperature profile along the heated axial length of the cladding, symmetric with respect to the tube mid-plane. The peak (mid-plane) temperature was varied at a constant rate to simulate the experimental conditions (Section 3.1.3). As for the pressure boundary conditions, constant pressure equal to the value of interest for the specific case was applied at the tube inner wall, with atmospheric pressure applied at the outer wall. Taking advantage of the symmetry of the problem, only the lower half of the heated cladding length was modeled in the 2D simulations. For the 3D simulation, a quarter of the cladding circumference was modeled. The combined overstress and overstrain criterion for cladding burst failure

Table 4
BISON separate-effects validation cases for cladding behavior under LOCA conditions.

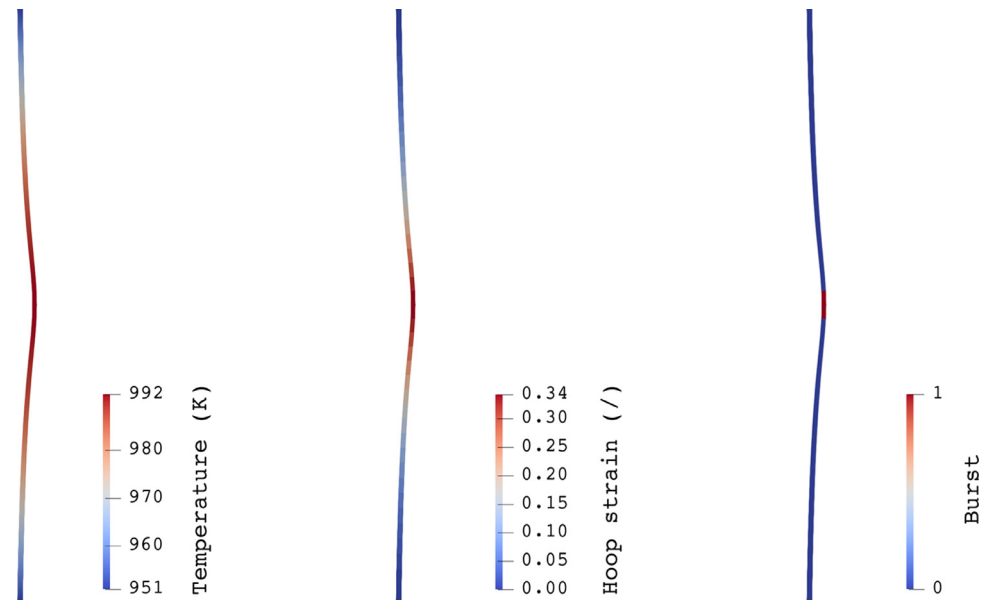| Experiment	Number of cases	Cladding material	Environment	Pressure range (MPa)	Temperature range (K)
REBEKA [4,11,12]	20	Zry-4	Steam	1-14	573-1310
PUZRY [13,14]	31	Zry-4	Argon	0.5-10	973-1473
Hardy [15]	16	Zry-4	Vacuum	0.3-13.8	600–1600
ORNL [16]	3	Zry-2 / Zry-4	Helium	6-9	380-1100
QUENCH-L1 [17]	2	Zry-4	Steam and argon	5.5-6	300-1470

Fig. 2. Contour plots of temperature, true hoop strain and location where the burst condition is attained for the BISON 2D simulation of the REBEKA test with 1 Ks^{-1} heating rate and 10 MPa internal pressure. Results are shown at the time of simulated cladding burst. Plots for the lower half of the heated cladding are mirrored to obtain a full-length view. The view is magnified 4 times in the radial direction for improved visualization.

(Section 2.4) was used. Note that the overstress failure criterion was developed based on experimental data from the REBEKA tests themselves [4]. Hence, the application of the combined overstress-overstrain criterion is expected to provide a meaningful assessment mostly of the strain limit.

3.1.3. 2D simulation results

Using 2D axisymmetric BISON models of the cladding tubes in the REBEKA tests, simulations were conducted considering various heating rates and inner cladding pressures to approximately represent the whole range of conditions of the experiments. In particular, peak temperature variation rates of 1, 10 and 30 Ks^{-1} were applied, and for each heating rate level, multiple levels of internal cladding pressure were considered to cover in detail the experimental range of 1 to 14 MPa. As a result, a total of 20 simulations were performed.

As an example of calculation results, Fig. 2 shows contour plots of temperature, true hoop strain and location where the condition for burst failure is attained for the case of 1 Ks^{-1} heating rate and 10 MPa internal pressure; results are shown at the time of simulated cladding burst. The cladding ballooning effect as reproduced by BISON is obvious.

Cladding burst failure is predicted at a temperature of about 990 K and a maximum true hoop strain of about 34%. Failure due to overstrain (Section 2.4) is predicted, with the strain limit being reached first in the mid-section of the cladding, where the temperature and creep rate are the highest. Hence, the value for the calculated maximum hoop strain at burst is largely determined by the limit on the permanent hoop strain included in the applied failure criterion.

The predictions of burst temperature for all of the considered heating rates and internal cladding overpressures are compared to the available experimental data in Fig. 3. The trends of increasing burst temperature with decreasing internal overpressure and with increasing heating rate are both reproduced qualitatively. Nevertheless, a systematic under-estimation of the burst temperature is observed. Moreover, higher discrepancies are noticed at the lower internal overpressure and heating rate levels. Discrepancies may be due to the uncertainties inherent in the cladding creep, oxidation and phase transformation models, and 3D effects (azimuthal tem-
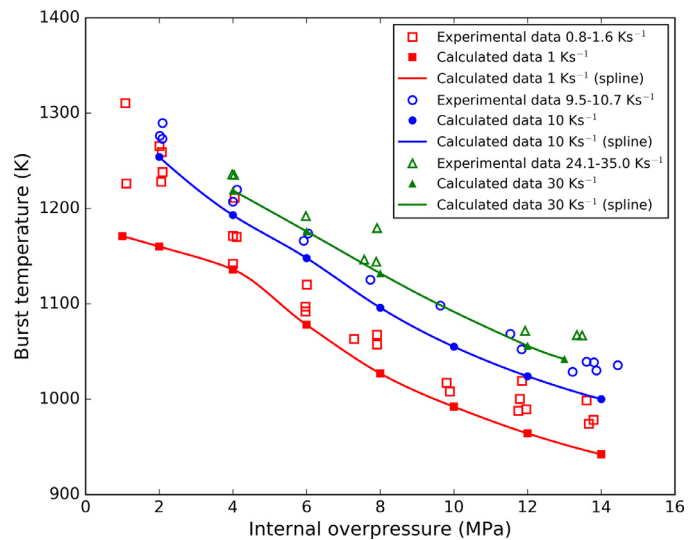

Fig. 3. Comparison between BISON calculations and experimental data of cladding burst temperature vs. internal overpressure for the simulations of the REBEKA tests. Internal overpressure is intended as the excess inner pressure relative to the outer pressure. Experimental data were digitized from [4]. Spline (Akima) interpolations of the calculated data are also included to provide visualization of the data trend.

perature differences) which cannot be captured in the current 2D representation.

Note that for the majority of the simulations, the limiting condition for the simulated burst failure turns out to be the overstrain criterion (Section 2.4). The only exceptions are the cases of 1 Ks^{-1} heating rate and 1, 2, 4 MPa internal pressure. Hence, the limiting strain assumption tends to be the most restrictive and the observed under-estimation of the cladding burst temperatures indicates that the BISON calculation tends to be conservative for these cases.

3.1.4. 3D simulation results

In the BISON 3D simulation, in addition to the above mentioned boundary conditions applied to the 2D simulations, an azimuthal
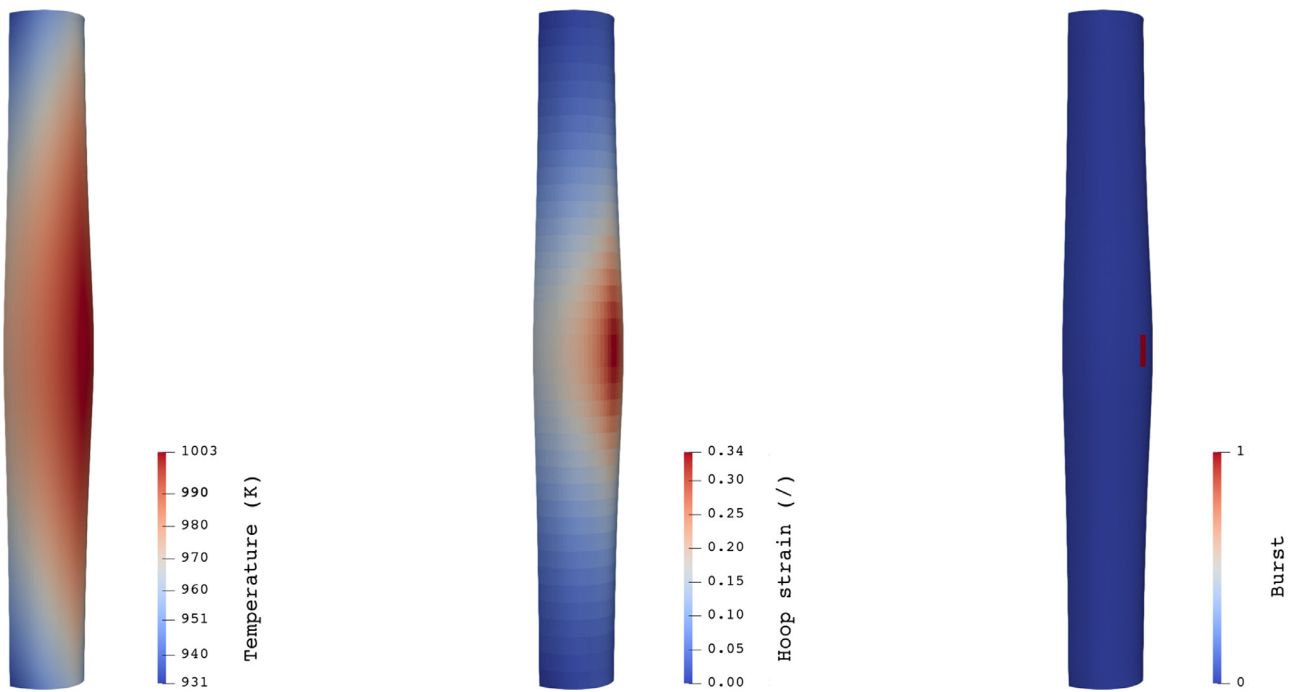
Fig. 4. Contour plots of temperature, true hoop strain and location where the burst condition is attained for the BISON 3D simulation of the REBEKA test with 1 Ks^{-1} heating rate and 10 MPa internal pressure. Results are shown at the time of simulated cladding burst. Plots for the lower quarter of the heated cladding are mirrored to obtain a full-length, half-circumference view. The view is magnified 4 times in the radial direction for improved visualization.

temperature gradient was included in the cladding temperature boundary condition. In particular, a maximum azimuthal temperature variation of 30 K was considered, which is realistic in light of the experimental indications available from thermocouple measurements in the REBEKA experiments [11,12]. The calculated results are presented for the exemplifying case of 1 Ks^{-1} heating rate and 10 MPa internal pressure at the time of cladding burst. Fig. 4 shows contour plots of temperature, true hoop strain and location where the condition for burst failure is attained. This 3D simulation had 19,612 degrees of freedom and was run in parallel on 8 processors with a run time of ~3.8 h. The simulation reproduces the non-uniform cladding ballooning and a localized burst on the hottest side of the cladding, which is consistent with the experimental observations [11,12]. Note that the burst temperature is higher (by about 10 K) than for the corresponding 2D simulation (Fig. 2), which indicates that capturing 3D aspects such as the effect of azimuthal temperature differences is of importance for fuel rod analysis during LOCA accidents. However, a more systematic work on 3D simulations of cladding ballooning to investigate the impact of azimuthal temperature variations on burst failure, including the effect on burst strain [11,12], is advisable before drawing more specific conclusions. Modeling the effect on burst strain may also require the development of a physically based burst failure criterion. Further investigation of 3D effects in fuel rod analysis during LOCAs with BISON will be pursued in the future.

3.2. PUZRY experimental series

The PUZRY experimental series [13,14] was carried out at AEKI, now Hungarian Academy of Sciences, Centre for Energy Research (MTA-EK), to study the mechanical behavior (ballooning and burst) of Zircaloy-4 cladding subject to inner pressure transients at high temperature that mimic LOCA conditions. In particular, the effects of temperature and pressurization rate on the deformation and the failure (burst) pressure were investigated. Some of the PUZRY tests were selected as priority cases within the IAEA FUMAC project [7].

3.2.1. Description of the tests

Thirty-one Zircaloy-4 tube samples were tested in a resistance furnace providing isothermal conditions in the temperature range of 973–1473 K. Specimens were 50 mm long cladding tubes placed in a quartz test tube filled with inert gas (argon) at a constant pressure of 0.1 MPa. The sample was pressurized from the inside with argon at a constant pressurization rate until burst of the tube occurred. Pressurization rates were between 7×10^{-4} and 2.6×10^{-2} MPa s^{-1}. The tube inner and outer diameters were 9.3 and 10.75 mm, respectively. The samples were closed with Zircaloy-4 end-plugs welded to the cladding.

3.2.2. Setup of BISON simulations

2D axisymmetric BISON models of the cladding tubes were built. Taking advantage of the axial symmetry of the problem, only the lower half of the heated cladding length was modeled. The presence of the end plugs was accounted for by applying zero radial displacement boundary conditions to the tube surfaces in correspondence of the plugs.

The furnace heating was simulated by a temperature boundary condition applied to the tube outer wall. Visual inspection of the tested specimens showed localized ballooning near the midplane [14], indicating a non-uniform temperature profile. Also, measurements performed in another furnace demonstrated an axial temperature variation of 6 K along the central 50-mm section of the furnace [36]. In view of this evidence, in the BISON simulations, a slight variation of the temperature along the tube length was applied. More in detail, a linear profile with a total variation of 6 K from tube end to mid-plane was considered, with the average temperature set equal to the experimental test temperature and the maximum temperature applied at the mid-plane.

Time-dependent pressures were simulated by pressure boundary conditions applied to the tube inner and outer walls. Prior to the pressure transient, the initial heat-up period was considered by applying atmospheric (0.1 MPa) pressure to both sides of the tube and ramping the temperature up from ambient (300 K) to the test
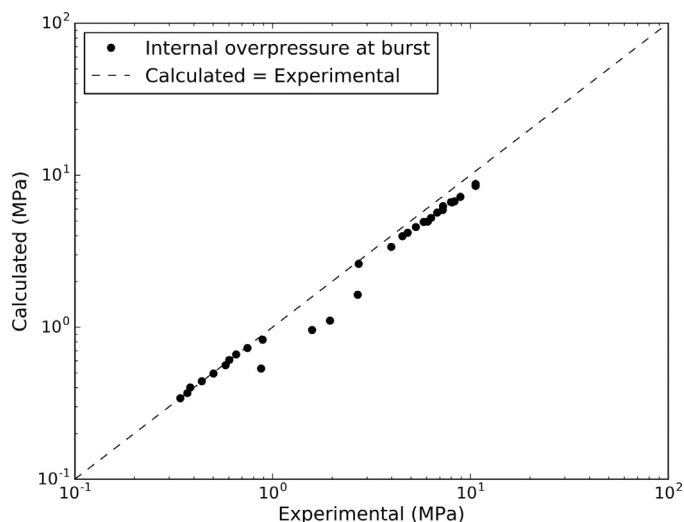
Fig. 5. Comparison of calculated and measured tube internal overpressure at burst for the PUZRY cases.
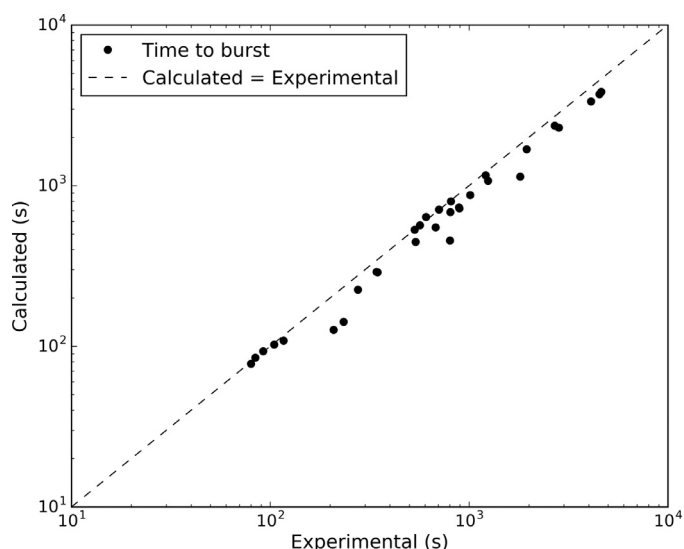

Fig. 6. Comparison of calculated and measured time to burst for the PUZRY cases.

temperature during 1000 s. Then, the inner pressure transient was applied, at constant temperature. The outer tube pressure was kept constant at 0.1 MPa.

3.2.3. Results

Figs. 5 and 6 show the comparisons between BISON calculations and experimental data of cladding internal overpressure at burst and time to burst, respectively, for the 31 PUZRY cases.

The accuracy of the BISON calculations appears reasonable. For all of the simulations, the limiting condition for the simulated burst failure is the overstrain criterion (Section 2.4). As with the REBEKA cases, the calculations tend to be conservative, with the calculated burst pressures and times being generally lower than the experimental values. Calculated and experimental burst times are also plotted as a function of test temperature in Fig. 7.

The decrease of the burst time with increasing test temperature is reproduced by the calculations. Deviations of calculated results from experimental data appear to be higher in the lower temperature region and in particular, below ~1050 K. This temperature approximately corresponds to the onset temperature of the α to β phase transformation of Zircaloy, noting that under isother-
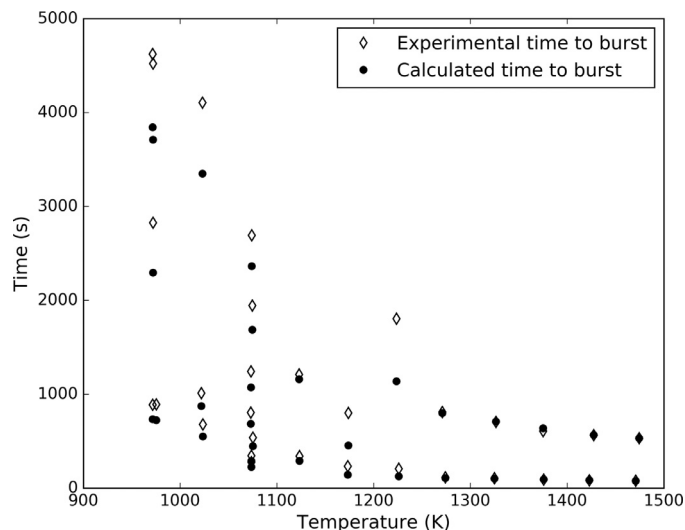

Fig. 7. Calculated and measured time to burst as a function of test temperature for the PUZRY cases.

mal conditions, the equilibrium curve is obeyed (Fig. 1). This indicates that discrepancies between calculations and experimental data may be partly due to anisotropic creep behavior, which characterizes α-Zircaloy [4,30] and is not considered in BISON at this time (see also Section 2.3). Discrepancies are also noticeable in the temperature range between approximately 1050–1250 K, i.e., the two-phase ($\alpha + \beta$) coexistence region at equilibrium (Fig. 1). In this regard, it has been observed that the largest uncertainty in the Zircaloy high-temperature creep correlation (Section 2.3) pertains to such two-phase coexistence domain of the alloy [37].

3.3. Hardy experimental series

The Hardy experiments [15] were designed to investigate the high-temperature strain and rupture behavior of Zircaloy-4 tubes in thermal-mechanical loading conditions representative of a LOCA. In particular, the effects of pressure and heating rate on the deformation and failure of the cladding tubes were investigated.

3.3.1. Description of the tests

The test technique involved heating of 500 mm long sections of cladding tubes in vacuum through an electrical current and at constant pressure. The cladding material was stress-relieved Zircaloy-4, having an outer diameter of 15.27 mm and a thickness of 380 μm. It has to be mentioned that tubes with these geometric characteristics are more representative of fuel cladding used in CANDU reactors than of LWR fuel cladding. Tubes were placed in an evacuated chamber and pressurized to various internal gas (helium) pressures. A heating rate of 25 Ks^{-1} or 100 Ks^{-1} was then imposed, rapidly increasing the tube temperature from 600 to 1600 K. Tests performed at tube internal pressures from 0.3 to MPa were considered for the simulations, i.e., all tests with available data in [15]. Burst temperature data were digitized from Figs. 6 and 7 in [15].

3.3.2. Setup of BISON simulations

A 2D axisymmetric finite element mesh was used to model the specimen tubes. Constant pressures consistent with the experimental conditions [15] were applied to the tube inner walls. Heating was simulated by a temperature boundary condition considering a slight variation of the temperature along the tube length. Similar to the simulations of the PUZRY cases (Section 3.2), a linear temperature profile with the maximum temperature at the tube
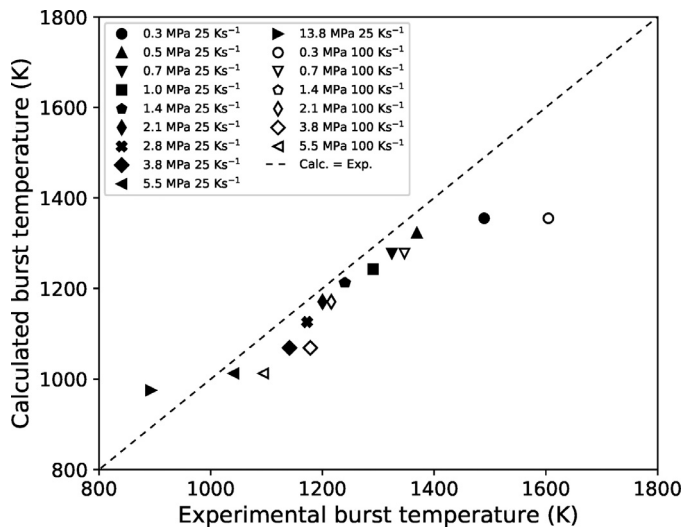
Fig. 8. Comparison of calculated and measured tube burst temperatures for the Hardy cases. The symbols corresponding to the two 1.4 MPa cases are superimposed in the plot.
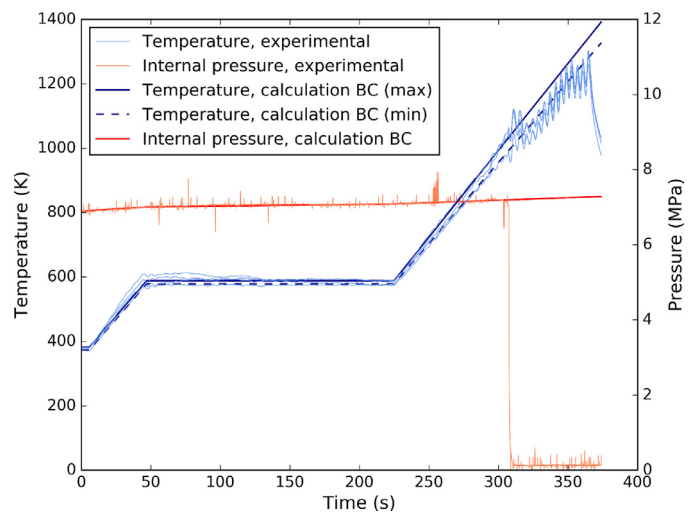

Fig. 9. Raw data of cladding temperature and inner pressure, and developed boundary conditions (BC) for the Zry4-1 test simulation. The experimental temperature includes recorded data from 4 thermocouples, all of which are included in the plot as the 4 light blue lines. As the purpose is limited to giving an account of the spread of the recorded temperatures, no explicit color distinction is made between curves corresponding to different thermocouples. (For interpretation of the references to color in this figure legend, the reader is referred to the web version of this article.)

mid-plane was considered. In the absence of specific indications, a total temperature variation of 1.5% (9–24 K) between the tube ends and mid-plane was applied as a preliminary approach.

3.3.3. Results

Comparison plots of computed versus measured burst temperatures are given in Fig. 8. The overall comparisons are reasonable. With the exception of the case with the highest inner cladding pressure of 13.8 MPa, BISON systematically under-estimates the burst temperature. This outcome is consistent with the tendency to provide conservative calculations for the time to burst observed for the REBEKA and PUZRY cases (Sections 3.1 and 3.2).

Also similar to the REBEKA and PUZRY cases, for the majority of the Hardy simulations, the limiting condition for burst failure turns out to be the overstrain criterion (Section 2.4). The only exceptions are the cases with 0.3 MPa internal pressure, for which the more restrictive condition is the overstress criterion.

3.4. ORNL experimental series

Experimental burst tests were performed at Oak Ridge National Laboratory (ORNL) on Zircaloy-2 and Zircaloy-4 cladding tubes pressurized internally with helium and subject to temperature transients that mimicked LOCA conditions [16]. In this Section, BISON simulations of selected tests from the ORNL campaign are presented.

3.4.1. Description of the tests

Cladding burst tests were carried out at ORNL's Severe Accident Test Station, inside the integral LOCA furnace module [16]. The experimental setup utilized an 8 kW infrared furnace to rapidly heat a 300 mm long, internally pressurized tube. The test configuration consisted of 8.2 mm diameter zirconia pellets inside a cladding tube of the material of interest. The loaded tube was centered inside a quartz furnace tube and had at least three Type-S thermocouples attached to its surface. The rod was internally pressurized with He while steam was continuously flowing at 0.1 MPa on the outside of the cladding. At the top, away from the heated zone, a miniature pressure transducer was attached to the rod to monitor the pressure inside the rod. The burst test sequence consisted of ramping at 5 Ks^{-1} from 573 to 1473 K, holding at 1473 K for 3 min, ramping down to 1073 K, and finally, quenching with room-temperature water.

Tests were performed for various cladding materials but in this work, we focus on the Zircaloy cases. The geometry of the cladding tubes examined in this study is reported in Table 5.

3.4.2. Setup of BISON simulations

BISON simulations were performed for one Zircaloy-4 test and two Zircaloy-2 tests. These represent the totality of the Zircaloy tests performed at ORNL with the exception of one Zircaloy-4 test for which the recorded temperature-pressure data will require further investigation. Finite-element 2D axisymmetric models of the cladding tubes were used. Assuming a symmetric problem with respect to the mid-plane, only the lower half of the heated cladding length was modeled. Actually, since the tests were performed in flowing superheated steam, the axial cladding temperature profile would be expected to be non-symmetric with respect to the mid-plane. However, due to the relatively small heat zone for the furnace and the relatively low initial temperature of the steam, in fact, the temperature was maximum near the tube mid-plane [38]. Therefore, the assumption of a symmetric temperature profile with respect to the mid-plane (see also Section 3.4.3) appears justified.

3.4.3. Boundary conditions development

The time-dependent temperatures and inner pressure for the cladding tubes were imposed as boundary conditions, whose values as a function of time were derived from thermocouple and pressure transducer data received from ORNL. In order to construct suitable noise-free boundary conditions for the BISON simulations, linear fits were made of the temperature and pressure signals. By way of example, Fig. 9 shows the time evolution of tube inner pressure and temperatures for the Zircaloy-4 case (referred to as test Zry4-1). Both raw signals and data fits used as BISON inputs are illustrated.

A separate fit was made for each of the test phases, which have approximately linear temperature/pressure evolutions, with continuity being imposed for the overall curves. For the temperature as a function of time, raw data from four thermocouples are given, and are plotted in Fig. 9. Differences in the signals from different thermocouples are noticeable, indicating that a significant axial temperature profile existed in the sample. Also, the maximum temperature was recorded at the thermocouples at the mid-

Table 5
Main cladding characteristics for the ORNL burst tests [16].

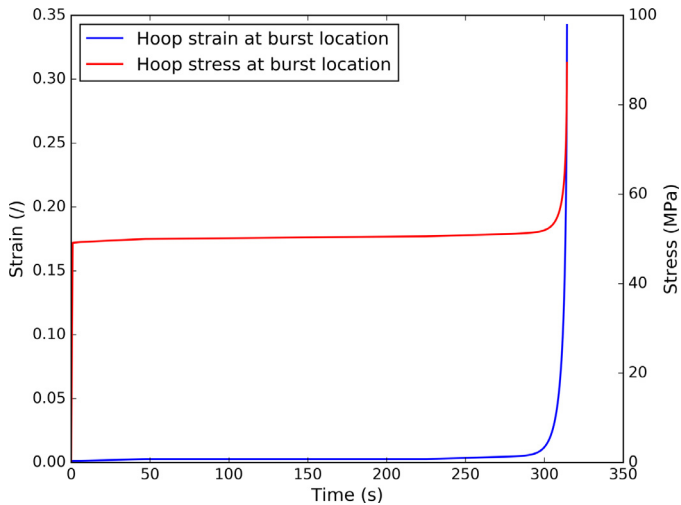| Alloy	Inner diameter (mm)	Outer diameter (mm)	Thickness (mm)	Length (mm)
Zircaloy-4	8.35	9.50	0.575	300
Zircaloy-2	9.75	11.16	0.705	300

Fig. 10. Time evolution of true hoop strain and hoop stress at the cladding outer surface at burst location for the Zry4-1 test simulation.

Table 6
Experimental and calculated time to burst for the ORNL burst tests simulated in this work.

Test label	Time to burst (s)		Burst temperature (K)	
	Exp.	Calc.	Exp.	Calc.
Zry4-1	307	314	1064	1071
Zry2-1	317	331	1010	1061
Zry2-2	437	448	1035	1110

plane [38]. In order to develop the temperature boundary conditions for the present simulations including a meaningful axial profile, the following approach was adopted. The fit of the maximum temperature data signal was used as the maximum, mid-plane temperature boundary condition ('max' in Fig. 9). An axial temperature profile with a peak at the mid-plane of the tube is also consistent with the cladding strain during the experiment showing an axial peak and burst occurring near the mid-plane [16]. A linear profile was considered along the axial direction, with the lower value estimated based on the lower recorded temperatures from the other thermocouples ('min' in Fig. 9). It can be observed in Fig. 9 that the linear fits used as BISON boundary conditions approximate the minimum and maximum temperatures recorded experimentally up to the time of rod burst (corresponding to the pressure drop), beyond which the noise in the experimental temperature signal increases significantly.

For the BISON boundary condition of cladding inner pressure, the linear fit for the pressure evolution during the heating transient was extrapolated beyond the time of rod burst, when the pressure in the experiment drops because of the burst opening. In this regard, for a meaningful simulation the pressure follows a realistic trend for an intact rod during the transient until the simulated time to burst, which may occur later than in the experiment. The outer pressure boundary condition is constant at ambient pressure throughout the simulation, consistent with the experimental conditions.

Boundary conditions for the Zircaloy-2 cases (referred to as Zry2-1 and Zry2-2) are qualitatively similar to the Zry4-1 case.

3.4.4. Results
Fig. 10 shows the time evolution of the calculated true hoop strain and hoop stress at the cladding outer surface at the burst location (mid-plane) for the Zry4-1 case. The cladding deforms outwards due to thermal creep under the tensile stress caused by the inner pressure and with the increasing temperature during the simulated test. Because of the exponential dependence of the ther-

mal creep rate on temperature (Section 2.3), the strain rate increases rapidly as burst failure is approached. Correspondingly, the stress increases with the increasing cladding radius and decreasing cladding thickness.

In the simulation, burst failure occurs at the attainment of the overstrain limit (Section 2.4) at ~314 s time, compared to an experimental value of approximately ~307 s. This is an accurate estimation considering the uncertainties and approximations in state-of-the-art modeling for LOCA conditions, as demonstrated by the recent IAEA FUMAC project [7,34]. Cladding temperature at burst location and time is ~1071 K, with the experimental value being ~1064 K.

Table 6 summarizes calculated and experimental values of time to burst for the ORNL burst tests simulated in this work. The calculation accuracy for the Zircaloy-2 cases also appears reasonable, although less accurate than for the Zry4-1 case. As with the Zircaloy-4 case, for both Zircaloy-2 simulations burst is due to overstrain. This outcome confirms that the limiting strain assumption tends to be more restrictive than the limiting stress assumption. Finally, it is noted that the calculated times to burst for the 3 ORNL burst tests considered here are later than the experimental values, hence, they are not conservative. This is a different outcome relative to the simulations of the REBEKA (Section 3.1), PUZRY (Section 3.2) and Hardy (Section 3.3) cases, and will require further investigation.

3.5. QUENCH-L1 experiment

The QUENCH-L1 experiment [17] was performed at Karlsruhe Institute of Technology (KIT) and consisted of multiple simulator rods within a bundle, tested under representative LOCA conditions. Among the objectives of the experiment was the investigation of cladding ballooning and burst behavior. The test rods consisted of Zircaloy-4 claddings containing annular ZrO_2 pellets as surrogate fuel, with heating achieved using electric heaters within the pellets. In this Section, BISON simulations of two of the QUENCH-L1 rods (i.e., rods 4 and 7) are presented. These rods were selected as priority cases within the IAEA FUMAC project, although only results for rod 4 where ultimately included [7].

3.5.1. Description of the test
During the QUENCH-L1 experiment, superheated steam and argon entered a test rod bundle at the bottom of the assembly and flowed upward. The argon, steam, and hydrogen produced through the zirconium-steam reaction exited through a water-cooled off-gas pipe to a condenser, separating steam from the argon and hydrogen. Quenching water was injected via an independent line at

the bottom of the assembly. The test bundle consisted of 21 fuel rod simulators and four corner rods. A shroud surrounded the bundle to simulate the adiabatic surrounding of a reactor core as well as guide steam and gas through the assembly. Each fuel rod simulator was approximately 2.5 m in length. The heated length of the rod consisted of a central tantalum heater surrounded by annular ZrO_2 pellets. The plenum separating the heater/pellet combination meant to simulate fuel pellets was filled with krypton gas with a gap between the outer radius of the ZrO_2 pellets and the cladding of 75 μm. A Zircaloy-4 cladding tube having an outer diameter of 10.75 mm and a thickness of 725 μm encased this system. The heated cladding length was 1024 mm. Thermocouples distributed along the cladding outer surface collected temperature data throughout the experiment. Pressure sensors in the plenum as well as the inlet and outlet of the test section recorded internal rod and system pressures, respectively.

The system pressure in the test section was about 0.3 MPa. The experiment began by applying a total power of 3.5 kW to the electrical bundle. Fuel rod simulators were then individually backfilled to 5.5 MPa and electrical power was rapidly increased to 43 kW to initiate the transient. This initial power increase was followed by a steady increase to 59 kW over the next 87 s. The power was then rapidly decreased back to 3.5 kW with water injection (quenching) beginning 207 s after the beginning of the transient heating phase.

3.5.2. Setup of BISON simulations

Rods 4 and 7 of the QUENCH-L1 experiment were chosen for consideration. Results from the instrumentation were used as applicable to define boundary conditions in the model. 2D axisymmetric finite element meshes were developed for this problem. For simplicity, only the heated length of the rods was represented in the BISON models.

The heater and pellets were modeled as two separate blocks with material properties of the ZrO_2 pellets obtained from [17].

To derive the heat source term applied in the simulation, data from [17] for the tantalum heaters were used. For the rod inner pressure boundary conditions, data from [17] were also digitized and used as input for the calculations. In the original data, the inner rod pressure drops at a certain time during the transient heating phase, indicating the point at which the cladding failed due to burst. For a meaningful simulation the input pressure history was set up to follow a realistic trend for an intact rod during the transient until the simulated time to burst, which may occur later than in the experiment. In particular, the pressure from the beginning of the transient until the experimental time to burst was fitted to a linear regression model, and this pressure model was used as the rod inner pressure boundary condition from time zero to the end of the simulation. As an example, the experimental data for the rod inner pressure and the fit used as boundary conditions for the BISON simulation of QUENCH-L1 rod 4 are shown in Fig. 11. Data for rod 7 are qualitatively similar and not shown here for brevity.

To obtain outer cladding temperature boundary conditions accurate to experimental conditions, cubic spline interpolation along the axial direction of the sampled cladding surface thermocouple data was performed. Rod 7 has the axial collection points required, but the lowest collection point for rod 4 is 25 mm above the bottom of the rod heated length. To remedy this gap in the data, we assumed that system conditions are similar for the two rods below the heated length, and added data from one thermocouple at the lower part of rod 7 to the rod 4 data. As an example, the data and interpolated values for rod 4 are plotted in Fig. 12 at several times during the transient heating phase.

To derive the boundary condition for the system pressure along the cladding, pressure values recorded over time and given in [17] were used. In particular, pressure data at the inlet and out-
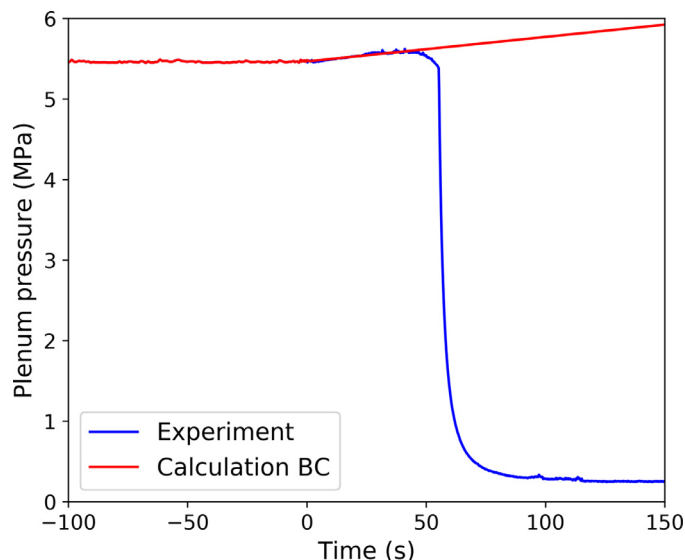

Fig. 11. Rod inner pressure experimental data vs. time and linear regression fit applied as boundary condition (BC) for the QUENCH-L1 rod 4 simulation. Time zero corresponds to the beginning of the transient heating phase.
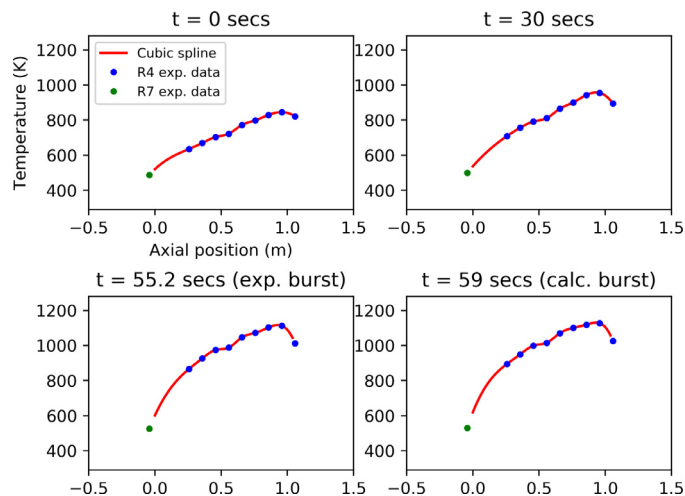

Fig. 12. Cladding outer temperature experimental data vs. axial position and cubic spline interpolation applied as boundary condition at various times for QUENCH-L1 rod 4. Axial position zero corresponds to the bottom of the heated length.

let of the test section were linearly interpolated axially and in time to produce the boundary conditions for the BISON calculations.

3.5.3. Results

To give an account of the kinetics involved in the simulated cladding ballooning process, Fig. 13 shows the calculated time evolution of the true hoop strain and temperature at peak locations for rod 4 during the heating phase of the experiment. Ballooning corresponds to the rapid acceleration of cladding strain due to thermal creep with increasing temperature. Rapid thermal creep and ballooning continue until failure due to burst occurs at the location of maximum strain. For both simulations, the limiting condition for burst failure is the overstrain criterion (Section 2.4).

Comparison of metrics between the experiment and calculations are provided in Table 7.

Cladding burst in the simulations occurs ~59 s and ~72 s after beginning the transient heating phase for rods 4 and 7, respectively. Both times are later than the experimental failures observed at ~55 s and ~60 s. As with the ORNL burst tests sim-
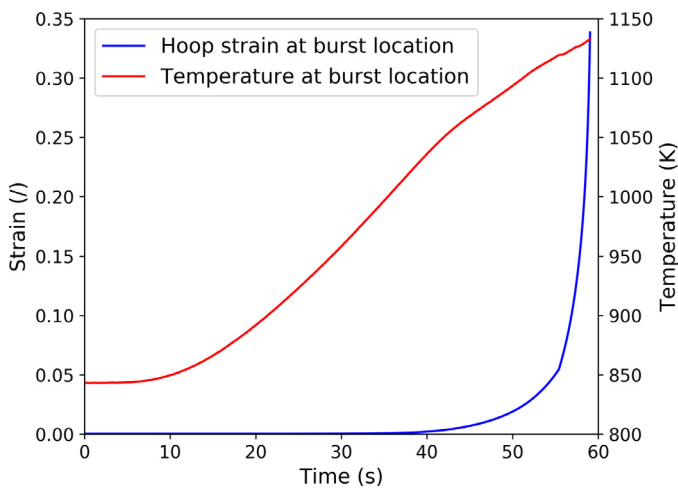
Fig. 13. Calculated true hoop strain and temperature at peak locations in the cladding from beginning of the heating phase until burst for the QUENCH-L1 rod 4 simulation.

Table 7
Experimental data (from [17]) and BISON simulation results for QUENCH L1 rods 4 and 7.

	Rod 4		Rod 7	
	Exp.	Calc.	Exp.	Calc.
Time to burst (s)	55	59	60	72
Burst pressure (MPa)	5.4	5.7	5.5	5.7
Burst temperature (K)	1154	1126	1074	1085
Burst elevation (mm)	979	928	953	795

ulations, the non-conservative character of the burst calculations for the QUENCH-L1 cases will require further investigation. Deviations of calculated results from experimental data may be partly due to 3D effects, which cannot be captured in the current 2D representation. In particular, azimuthal temperature variations in the cladding have been observed during the QUENCH-L1 experiment [17]. As discussed in Section 3.1.4, accounting for the effect of azimuthal temperature variations through 3D modeling is potentially of importance to the accurate simulation of cladding ballooning and burst behavior under LOCA conditions, and further work on this subject is advisable. Calculated results of cladding temperature and inner pressure at burst are in reasonably good agreement with the measured values. Burst elevations for both simulations are lower than the experimental locations, but are consistent with the experiment in that burst failure occurs at the upper end of the fuel rod simulators.

4. Conclusions

We presented modeling developments of the BISON fuel performance code for the analysis of Zircaloy cladding behavior during LOCA accident scenarios and code validation to cladding ballooning and burst experimental tests. BISON developments included models for cladding high-temperature steam oxidation, crystallographic phase transition, high-temperature creep and failure due to burst. The implemented models are mostly based on data relative to Zircaloy-4. However, it is generally accepted that Zircaloy-2 exhibits a very similar behavior to Zircaloy-4 in the high temperature range relevant to the considered phenomena. Accordingly, the performed developments are deemed applicable to cladding behavior analysis for both alloys. A total of 72 cladding tests from the REBEKA, PUZRY, Hardy, ORNL and QUENCH-L1 experiments were simulated and calculations were compared to experimen-

tal data for code validation. All simulated tests were performed on fresh Zircaloy-2/4 claddings. The BISON calculations were constructed with imposed temperature and pressure boundary conditions based on the available measured data. All simulations were performed using 2D axisymmetric models. For one of the REBEKA cases, however, we also presented a 3D calculation that demonstrated simulation of the cladding response in presence of azimuthal temperature variations. In general, the BISON calculations for cladding burst temperature, inner pressure at burst and time to burst compared adequately to the experimental data. More precisely, the overall accuracy of the BISON calculations appears in line with the state of the art when assessed in relation to the recent results of the IAEA FUMAC project [7]. Among the open issues that were identified as potential reasons for the observed discrepancies between calculations and experimental data are (i) uncertainties associated with the correlation for cladding high-temperature creep, (ii) anisotropic creep behavior, which is currently not considered in the computational model, and (iii) uncertainties associated with the choice of the cladding burst failure criterion. In this connection, for the vast majority of the performed simulations, the limiting strain criterion for the determination of the cladding burst condition was found to be more restrictive than the limiting stress criterion.

Simulation of separate-effects cladding experiments was aimed to assess cladding models decoupled from complexities related to modeling fuel behavior and the associated uncertainties. The work presented in this paper therefore provides the basis for application of the BISON code to integral fuel rod simulations for LOCA scenarios as a next step. A complementary paper [18] deals with BISON modeling developments for fuel behavior and simulation of integral fuel rod LOCA experiments.

Data availability

The data generated during the current study are available from the authors on request, subject to approval for release by INL.

Declaration of Competing Interest

The authors declare that they have no known competing financial interests or personal relationships that could have appeared to influence the work reported in this paper.

References

[1] P. Van Uffelen, C. Győri, A. Schubert, J. van de Laar, Z. Hoózer, G. Spykman, Extending the application range of a fuel performance code from normal operating to design basis accident conditions, J. Nucl. Mater. 383 (2008) 137–143.

[2] P. Van Uffelen, J. Hales, W. Li, G. Rossiter, R. Williamson, A review of fuel performance modelling, J. Nucl. Mater. 516 (2019) 373–412.

[3] P. Van Uffelen, G. Pastore, Oxide fuel performance modeling and simulation, in: R. Konings, R.E. Stoller (Eds.), Comprehensive Nuclear Materials, Elsevier, 2020.

[4] F.J. Erbacher, H.J. Neitzel, H. Rosinger, H. Schmidt, K. Wiehr, Burst criterion of Zircaloy fuel claddings in a loss-of-coolant accident, in: D.G. Franklin (Ed.), Proceedings of the Fifth Conference on Zirconium in the Nuclear Industry, American Society for Testing and Materials, 1982, pp. 271–283. ASTM STP 754

[5] M.S. Veshchunov, A.V. Boldyrev, V.D. Ozrin, V.E. Shestak, V.I. Tarasov, A new mechanistic code SFPR for modeling of single fuel rod performance under various regimes of LWR operation, Nucl. Eng. Des. 241 (2011) 2822–2830.

[6] A. Prudil, B.J. Lewis, P.K. Chan, J.J. Baschuk, D. Wowk, Development and testing of the FAST fuel performance code: transient conditions (Part 2), Nucl. Eng. Des. 282 (2015) 169–177.

[7] Fuel Modelling in Accident Conditions (FUMAC): Final Report of a Coordinated Research ProjectTechnical Report IAEA-TECDOC-1889, International Atomic Energy Agency, 2019.

[8] R.L. Williamson, J.D. Hales, S.R. Novascone, M.R. Tonks, D.R. Gaston, C.J. Permann, D. Andrs, R.C. Martineau, Multidimensional multiphysics simulation of nuclear fuel behavior, J. Nucl. Mater. 423 (2012) 149–163.

[9] J.D. Hales, S.R. Novascone, B. Spencer, R.L. Williamson, G. Pastore, D.M. Perez, Verification of the BISON fuel performance code, Ann. Nucl. Energy 71 (2014) 81–90.

[10] R.L. Williamson, K.A. Gamble, D.M. Perez, S.R. Novascone, G. Pastore, R.J. Gardner, J.D. Hales, W. Liu, A. Mai, Validating the BISON fuel performance code to integral LWR experiments, Nucl. Eng. Des. 301 (2016) 232–244.

[11] M.E. Markiewicz, F. Erbacher, Experiments on Ballooning in Pressurized and Transiently Heated Zircaloy-4 Tubes, Technical Report KfK 4343, Kernforschungszentrum Karlsruhe, Germany, 1988.

[12] F. Erbacher, H. Neitzel, K. Wiehr, Cladding Deformation and Emergency Core Cooling of a Pressurized Water Reactor in a LOCA. Summary Description of the REBEKA Program, Technical Report KfK 4781, Kernforschungszentrum Karlsruhe, Germany, 1990.

[13] E. Perez-Feró, C. Győri, L. Matus, L. Vasáros, Z. Hózer, P. Windberg, L. Maróti, M. Horváth, I. Nagy, A. Pintér-Csordás, T. Novotny, Experimental database of E110 claddings exposed to accident conditions, J. Nucl. Mater. 397 (2010) 48–54.

[14] E. Perez-Feró, Z. Hózer, T. Novotny, G. Kracz, M. Horváth, I. Nagy, A. Vimi, A. Pintér-Csordás, C. Győri, L. Matus, L. Vasáros, P. Windberg, L. Maróti, Experimental Database of E110 Claddings under Accident Conditions, Technical Report EK-FRL-2012-255-01/02, Center for Energy Research, Hungarian Academy of Sciences, Budapest, Hungary, 2013.

[15] D. Hardy, High temperature expansion and rupture behaviour of Zircaloy tubing, in: Proceedings of the CSNI Specialist Meeting on Safety of Water Reactor Fuel Elements,Saclay, France, 1973.

[16] C.P. Massey, K.A. Terrani, S.N. Dryepondt, B.A. Pint, Cladding burst behavior of Fe-based alloys under LOCA, J. Nucl. Mater. 470 (2016) 128–138.

[17] J. Stuckert, M. Große, C. Rössger, M. Steinbrück, M. Walter, Results of the LOCA Reference Bundle Test QUENCH-L1 with Zircaloy-4 Claddings, Technical Report KIT-SR 7651, Karlsruher Institut für Technologie, Germany, 2015.

[18] G. Pastore, K.A. Gamble, R.L. Williamson, S.R. Novascone, R.J. Gardner, J.D. Hales, Analysis of fuel rod behavior during loss-of-coolant accidents using the BISON code: Fuel modeling developments and simulation of integral experiments, J. Nucl. Mater. (2020). Submitted to.

[19] G. Schanz, Recommendations and Supporting Information on the Choice of Zirconium Oxidation Models in Severe Accident Codes, Technical Report FZKA 6827, SAM-COLOSS-P043, Forschungszentrum Karlsruhe, Germany, 2003.

[20] S. Leistikow, G. Schanz, H.V. Berg, A. Aly, Comprehensive presentation of extended Zircaloy-4/steam oxidation results 600-1600 C, in: Proceedings of CSNI/IAEA Specialists Meeting on Water Reactor Fuel Safety and Fission Product Release in Off-normal and Accident Conditions, Risø National Laboratory, Denmark, 1983.

[21] J.V. Cathcart, R.E. Pawel, R.A. McKee, R.E. Druschel, G.J. Yurek, J.J. Campbell, S.H. Jury, Zirconium Metal-water Oxidation Kinetics, IV. Reaction Rate Studies, Technical Report ORNL/NUREG-17, Oak Ridge National Laboratory, USA, 1977.

[22] J.T. Prater, E.L. Courtright, Zircaloy-4 Oxidation at 1300 to 2400 C, Technical Report NUREG/CR-4889, PNL-6166, Pacific Northwest National Laboratory, USA, 1987.

[23] F. Garzarolli, W. Jung, H. Shoenfeld, A.M. Garde, G.W. Parray, P. Smerd, Review of PWR Fuel Rod Waterside Corrosion Behavior, Technical Report EPRI NP-2789, Electric Power Research Institute, Palo Alto, CA, USA, 1982.

[24] F. Garzarolli, M. Garzarolli, PWR Zr Alloy Cladding Water Side Corrosion – State of Knowledge on in-PWR Corrosion Analysis Methods of Measured Oxide Data and Oxide Thickness Prediction, 2012, (Advanced Nuclear Technology International, Mölnlycke, Sweden).

[25] N. Möes, J. Dolbow, T. Belytschko, A finite element method for crack growth without remeshing, Int. J. Numer. Methods Eng. 46 (1999) 131–150.

[26] W. Jiang, B.W. Spencer, J.E. Dolbow, Ceramic nuclear fuel fracture modeling with the extended finite element method, Eng. Fract. Mech. 223 (2020) 106713.

[27] A.R. Massih, Transformation kinetics of zirconium alloys under non-isothermal conditions, J. Nucl. Mater. 384 (2009) 330–335.

[28] A.R. Massih, L.O. Jernkvist, Transformation kinetics of alloys under non-isothermal conditions, Model. Simul. Mater. Sci. Eng. 17 (2009) 055002.

[29] T. Manngård, L.O. Jernkvist, A.R. Massih, Evaluation of Loss-of-Coolant Accident Simulation Tests with the Fuel Rod Analysis Code FRAPTRAN-1.4, Technical Report TR11-008V1, Quantum Technologies AB, Sweden, 2011.

[30] H.J. Neitzel, H. Rosinger, The Development of a Burst Criterion for Zircaloy Fuel Cladding Under LOCA Conditions, Technical Report KfK 4343, Kernforschungszentrum Karlsruhe, Germany, 1980.

[31] W. Liu, J. Rashid, D. Sunderland, Numerical method of modeling creep of zirconium-alloy cladding in a multi-physics fuel performance code, in: Proceedings of the International Conference on Water Reactor Fuel Performance – Top Fuel, Charlotte, NC, USA, September 15-19, 2013.

[32] V. Di Marcello, A. Schubert, J. van de Laar, P. Van Uffelen, The TRANSURANUS mechanical model for large strain analysis, Nucl. Eng. Des. 276 (2014) 19–29.

[33] BISON Code Documentation, (https://mooseframework.org/bison/syntax/bison_only_index.html), 2020.

[34] G. Pastore, K. Kulacsy, IAEA FUMAC benchmark of fuel performance codes based on LOCA separate-effects cladding tests, in: Proceedings of the Reactor Fuel Performance Meeting – Top Fuel, Prague, Czech Republic, September 30–October 4, 2018.

[35] Y. He, K. Shirvan, Y. Wu, G. Su, Integrating a multi-layer deformation model in FRAPTRAN for accident tolerant fuel analysis, Ann. Nucl. Energy 133 (2019) 441–454.

[36] K. Kulacsy, (Center for Energy Research, Hungarian Academy of Sciences, Communication within the FUMAC project), March (2015).

[37] T. Manngård, A.R. Massih, Modelling and simulation of reactor fuel cladding under loss-of-coolant accident conditions, J. Nucl. Sci. Technol. 48 (2011) 39–49.

[38] C.P. Massey, (Oak Ridge National Laboratory, Personal communication), August 2020.